catalysts

MDPI

Article

The Effect of ZrO_2 as Different Components of Ni-Based Catalysts for CO_2 Reforming of Methane and Combined Steam and CO_2 Reforming of Methane on Catalytic Performance with Coke Formation

Wassachol Sumarasingha [1,2], Somsak Supasitmongkol [3] and Monrudee Phongaksorn [1,2,*]

[1] Department of Industrial Chemistry, Faculty of Applied Science, King Mongkut's University of Technology North Bangkok, Bangkok 10800, Thailand; w.sumarasingha@gmail.com
[2] Research and Development Center for Chemical Engineering Unit Operation and Catalyst Design (RCC), King Mongkut's University of Technology North Bangkok, Bangkok 10800, Thailand
[3] National Energy Technology Center (ENTEC), National Science and Technology Development Agency (NSTDA), 111 Thailand Science Park, Phahonyothin Road, Klong 1, Klong Luang, Pathum Thani 12120, Thailand; somsak.sup@entec.or.th
* Correspondence: monrudee.p@sci.kmutnb.ac.th; Tel.: +66-255-52000 (ext. 4822)

Abstract: The role of ZrO_2 as different components in Ni-based catalysts for CO_2 reforming of methane (CRM) has been investigated. The 10 wt.% Ni supported catalysts were prepared with ZrO_2 as a support using a co-impregnation method. As a promoter (1 wt.% ZrO_2) and a coactive component (10 wt.% ZrO_2), the catalysts with ZrO_2 were synthesized using a co-impregnation method. To evaluate the effect of the interaction, the Ni catalyst with ZrO_2 as a coactive component was prepared by a sequential impregnation method. The results revealed that the activity, the selectivity, and the anti-coking ability of the catalyst depend upon the ZrO_2 content, the Ni-ZrO_2 interaction, basicity, and oxygen mobility of each catalyst resulting in different Ni dispersion and oxygen transfer pathway from ZrO_2 to Ni. According to the characterization and catalytic activation results, the Ni catalyst with low ZrO_2 content (as a promoter) presented highest selectivity toward CO owning to the high number of weak and moderate basic sites that enhance the CO_2 activation-dissociation. The lowest activity (CH_4 conversion ≈ 40% and CO_2 conversion ≈ 39%) with the relatively high quantity of total coke formation (the weight loss of the spent catalyst in TGA curve ≈ 22%) of the Ni catalyst with ZrO_2 as a support is ascribed to the lowest Ni dispersion due to the poor Ni-ZrO_2 interaction and less oxygen transfer from ZrO_2 to the deposited carbon on the Ni surface. The effect of a poor Ni-ZrO_2 interaction on the catalytic activity was deducted by decreasing ZrO_2 content to 10 wt.% (as a coactive component) and 1 wt.% (as a promoter). Although Ni catalysts with 1 wt.% and 10 wt.% ZrO_2 provided similar oxygen mobility, the lack of oxygen transfer to coke during CRM process on the Ni surface was still indicated by the growth of carbon filament when the catalyst was prepared by co-impregnation method. When the catalyst was prepared by a sequential impregnation, the intimate interaction of Ni and ZrO_2 for oxygen transfer was successfully developed through a ZrO_2-Al_2O_3 composite. The interaction in this catalyst enhanced the catalytic activity (CH_4 conversion ≈ 54% and CO_2 conversion ≈ 50%) and the oxygen transport for carbon oxidation (the weight loss of the spent catalyst in TGA curve ≈ 7%) for CRM process. The Ni supported catalysts with ZrO_2 as a promoter prepared by co-impregnation and with ZrO_2 as a coactive component prepared by a sequential impregnation were tested in combined steam and CO_2 reforming of methane (CSCRM). The results revealed that the ZrO_2 promoter provided a greater carbon resistance (coke = 1.213 mmol·g^{-1}) with the subtraction of CH_4 and CO_2 activities (CH_4 conversion ≈ 28% and CO_2 conversion ≈ %) due to the loss of active sites to the H_2O activation-dissociation. Thus, the H_2O activation-dissociation was promoted more efficiently on the basic sites than on the vacancy sites in CSCRM.

Keywords: catalytic reforming; syngas; ZrO_2 content; Ni-ZrO_2 interaction; oxygen mobility; coke formation

check for updates

Citation: Sumarasingha, W.; Supasitmongkol, S.; Phongaksorn, M. The Effect of ZrO_2 as Different Components of Ni-Based Catalysts for CO_2 Reforming of Methane and Combined Steam and CO_2 Reforming of Methane on Catalytic Performance with Coke Formation. *Catalysts* **2021**, *11*, 984. https://doi.org/10.3390/catal11080984

Academic Editors: Rei-Yu Chein and Wei-Hsin Chen

Received: 16 July 2021
Accepted: 15 August 2021
Published: 17 August 2021

1. Introduction

Among the different routes for CO_2 utilization, CO_2 reforming of methane (CRM) is regarded as one of the most beneficial reactions for energy and environment. This reaction converts CO_2 and CH_4, the main greenhouse gases (GHGs), into a synthesis gas, a mixture of CO and H_2 (R1) [1,2]. The synthesis gas can be used as a fuel or a source of high value-added chemicals such as oxygenated derivatives (e.g., methanol) and synthetic fuels (via the Fischer–Tropsch (FT) process) [3–5]. Because CRM is a highly endothermic reaction, it is usually operated at temperature range of 650 °C to 1000 °C [6,7]. A high temperature causes the short life of Ni-based catalysts mainly due to the metal sintering and the carbon formation, a by-product from side reactions including the Boudouard reaction (R2) and CH_4 decomposition (R3) [8,9]. Additionally, reverse water gas shift (RWGS) reaction (R4) is an another endothermic side reaction that decrease the hydrogen yield [10–12]. To avoid catalyst deactivation via carbon deposition during CRM process, adding steam into the feed has been applied in order to raise the rate of coke oxidation [13]. Thus, the combined steam and CO_2 reforming of methane (CSCRM) (R5) has been considered as a better promising technique for a synthesis gas production. Therefore, CSCRM combines between CO_2 reforming and steam reforming of methane (SRM) (R6) in a single process. However, this process may cause an over expected energy consumption because of the evaporation of a high water quantity. Hence, the optimum steam content in the feed should be concerned in term of the coke resistance as well as the energy balance [14–16].

$$CH_4(g) + CO_2(g) \rightarrow 2H_2(g) + 2CO(g) \qquad \Delta H^\circ{}_{298} = +247\ kJ/mol \tag{R1}$$

$$2CO(g) \rightarrow CO_2(g) + C(s) \qquad \Delta H^\circ{}_{298} = -173\ kJ/mol \tag{R2}$$

$$CH_4(g) \rightarrow 2H_2(g) + C(s) \qquad \Delta H^\circ{}_{298} = +75\ kJ/mol \tag{R3}$$

$$CO_2(g) + H_2(g) \rightarrow CO(g) + H_2O(g) \qquad \Delta H^\circ{}_{298} = +41\ kJ/mol \tag{R4}$$

$$3CH_4(g) + 2H_2O(g) + CO_2(g) \rightarrow 8H_2(g) + 4CO(g) \qquad \Delta H^\circ{}_{298} = +712\ kJ/mol \tag{R5}$$

$$CH_4(g) + H_2O(g) \rightarrow 3H_2(g) + CO(g) \qquad \Delta H^\circ{}_{298} = +206\ kJ/mol \tag{R6}$$

In general, Ni-based catalysts are considered as the most practical catalysts for the CRM and CSCRM processes because of their cost-effective and high catalytic performance comparable to precious metal catalysts [10,16]. As it was mentioned, Ni-based catalysts are prone to deactivating by the sintering and the carbon deposition. Therefore, the development of Ni-based catalysts has become the main strategy for the commercialized CRM process. The well-dispersed Ni nanoparticles on the catalyst surface significantly resist the metal sintering and suppress the carbon deposition. An effective method for preventing surface carbon is to create oxygen mobility in Ni-based catalysts. Because the oxygen vacancies play an important role in generating the oxygen mobility of the catalyst, oxygen storage materials have been used as a component of Ni supported catalysts for this purpose. Zirconium oxide (ZrO_2) has been considered as the practical oxygen storage material due to its oxygen storage capacity, the acid-base bifunctional properties, the mechanical strength, and the high thermal stability [17–19]. The ZrO_2 promoter decreased the Ni-Al_2O_3 interaction in the Ni/Al_2O_3 catalyst [20–22]. Adding high ZrO_2 content, compared to low ZrO_2 content, enhanced the activity and stability of Ni-based catalysts since the oxygen vacancies of the ZrO_2 surface absorbed and stored more oxygen from the dissociation of CO_2 molecule, thereby improving the reforming activity and the oxidizing carbon deposits on the active surface [21,23]. The ZrO_2 support displayed a limitation in the specific surface area [24–27]. The different preparation methods of catalysts are widely examined in the literature. Such favourite methods as co-impregnation and sequential impregnation method were found that the ZrO_2-Ni/Al_2O_3 catalysts prepared via sequential impregnation demonstrated a greater catalytic performance and coke inhibition for a dry reforming reaction and CO methanation reaction [22,28]. In CSCRM process, several works reported that the ZrO_2 addition to Ni-based catalysts was employed to enhance

the oxygen storage capacity of ZrO_2, the redox property, and the promotion of metal dispersion. Additionally, the ZrO_2 improves the adsorption of steam onto the surface and activates the gasification of carbon deposited, reflecting an increase in H_2 production with a protection against a deposited carbon on Ni-based catalysts [29–31]. Although certain studies reported the effect of ZrO_2 as a different component, the role of them derived from their physicochemical properties that related to the CRM and CSCRM performances of Ni catalysts are required to be more clarified under the precisely similar condition. These relations can fulfil the detail of catalyst design for methane reforming processes.

This research reveals the linkage of ZrO_2 role in various components of the Ni supported catalysts and catalytic performances based upon characterization results accompanied with the CRM and CSCRM reaction data under the similar condition. In this paper, components of ZrO_2 that are not a support have been assigned by its content. According to the literature [32], promoters are defined as a substance added to heterogeneous catalysts in amounts of a few percent to rise the catalytic performances of a catalyst, and promoter loading in many works was not greater than 5%. Consequently, 1 wt.% ZrO_2 is assigned as a promoter. Because CO_2, a reactant of CRM reaction, can be adsorbed and activated at vacancies on ZrO_2, ZrO_2 at similar loading to the main active species, it is thus considered as a coactive component. As a support, the ZrO_2 was synthesized using the precipitation method, and the 10 wt.% Ni/ZrO_2 catalyst was prepared using the impregnation method. As a promoter, 1 wt.% ZrO_2 was co-impregnated with 10 wt.% Ni onto the Al_2O_3 support. As a coactive component, 10 wt.% ZrO_2 was loaded with 10 wt.% Ni onto the Al_2O_3 support using co-impregnation and the sequential impregnation method to generate the different interactions of Ni-ZrO_2 on the prepared catalysts. Physicochemical properties of these catalysts were comprehensively characterized by X-ray diffraction (XRD), N_2 adsorption–desorption, the temperature-programmed desorption of hydrogen (H_2-TPD), the temperature-programmed reduction of hydrogen (H_2-TPR), the temperature-programmed desorption of carbon dioxide (CO_2-TPD) and the temperature-programmed desorption of oxygen (O_2-TPD). The CRM activities of all catalysts were evaluated in a tubular fixed-bed reactor at 620 °C under atmospheric pressure for 10 h. Then, catalysts from this set were chosen for studying the effect of steam using CSCRM process that was tested in the similar condition with the additional steam into the feed. After the tests, the coke deposited on spent catalysts was determined employing thermal gravimetric analysis (TGA) for catalysts from CRM and the temperature-programmed oxidation (TPO) for catalysts from CSCRM. Then, this study identified the relation between the role of ZrO_2 as each component in the Ni supported catalysts and their reforming performances of methane. This study assists in further Ni-based catalysts development.

2. Results and Discussion

2.1. XRD Analysis and H_2-Temperature Programmed Desorption

The X-ray diffractograms of the reduced catalysts are displayed in Figure 1. The peaks of the tetragonal ZrO_2 phases at 2θ of 30.3°, 35.2°, 50.2°, and 60.2° (JCPDS 27-997) with the peaks of monoclinic ZrO_2 phases at 2θ of 24.1°, 28.3°, 31.5°, 34.2°, and 50.4° (JCPDS 37-1484) were only observed in the diffractograms of the reduced 10Ni/ZrO_2 catalyst [33]. The XRD patterns of the ZrO_2 were not detectable in the reduced 10Ni-xZrO_2/Al_2O_3 catalysts. In the diffractograms of the reduced 10Ni-xZrO_2/Al_2O_3 catalysts, three board peaks at 2θ of 37.0°, 43.1°, and 62.6° are ascribed to γ-Al_2O_3 phase (JCPDS No. 50-0741), overlapping with the peak pattern of the $NiAl_2O_4$ spinel structure (JCPDS No. 78-0552). The diffractograms of all catalysts showed peaks of the Ni crystalline phase at 2θ of 37.5°, 45.6°, and 66.6° (JCPDS No. 73-1519). For a quantitative comparison, the Ni particle size and the percentage metal dispersion calculated from the H_2-TPD results are included in Table 1. The Ni particle sizes on 10Ni/ZrO_2, 10Ni-1ZrO_2/Al_2O_3 (CI), 10Ni-10ZrO_2/Al_2O_3 (CI), and 10Ni-10ZrO_2/Al_2O_3 (SI) catalysts were estimated as 21.5, 7.8, 8.9, and 6.3 nm, respectively. The largest Ni particle sizes with the lowest metal dispersion of 3.0% were found in the 10Ni/ZrO_2 catalyst, representing the weak metal-support interaction because

of the poor interaction between Ni and ZrO_2 [34]. The 10Ni-xZrO_2/Al_2O_3 (CI) catalysts prepared by the co-impregnation method provided smaller Ni particle sizes with the greater metal dispersion compared to the 10Ni/ZrO_2 catalyst. The Ni particle sizes in the 10Ni-xZrO_2/Al_2O_3 (CI) catalysts diminished when the ZrO_2 content decrease, indicating a stronger metal-support interaction. Although the 10Ni-10ZrO_2/Al_2O_3 (SI) and 10Ni-10ZrO_2/Al_2O_3 (CI) catalyst have similar ZrO_2 proportion, the 10Ni-10ZrO_2/Al_2O_3 (SI) catalyst prepared by sequential impregnation exhibited the highest dispersion, resulting in the smallest Ni particle sizes and suggesting a strongest Ni-support interaction.

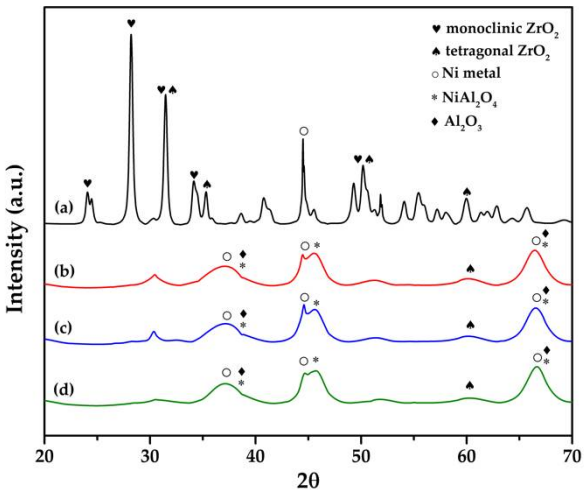

Figure 1. The X-ray diffraction patterns of the reduced (**a**) 10Ni/ZrO_2 (**b**) 10Ni-1ZrO_2/Al_2O_3 (CI), (**c**) 10Ni-10ZrO_2/Al_2O_3 (CI), and (**d**) 10Ni-10ZrO_2/Al_2O_3 (SI).

Table 1. Bulk and surface properties of Al_2O_3 support, ZrO_2 support, 10Ni/ZrO_2, 10Ni-1ZrO_2/Al_2O_3 (CI), 10Ni-10ZrO_2/Al_2O_3 (CI), and 10Ni-10ZrO_2/Al_2O_3 (SI).

Samples	N_2 Adsorption-Desorption		H_2-TPD	
	Surface Area ($m^2 \cdot g^{-1}$)	Total Pore Volume ($cm^3 \cdot g^{-1}$)	Ni Dispersion (%)	Ni Particle Size (nm)
Al_2O_3 support	165	0.20	-	-
ZrO_2 support	95	0.21	-	-
10Ni/ZrO_2	75	0.16	3.0	21.5
10Ni-1ZrO_2/Al_2O_3 (CI)	153	0.21	8.1	7.8
10Ni-10ZrO_2/Al_2O_3 (CI)	134	0.20	7.1	8.9
10Ni-10ZrO_2/Al_2O_3 (SI)	112	0.20	10.0	6.3

2.2. N_2 Adsorption-Desorption

N_2 adsorption-desorption isotherms and pore size distributions of calcined catalysts are presented in Figure 2 and the textural properties are reported in Table 1. All recorded isotherms (Figure 2a) depicted the type IV isotherm features of mesoporous materials with an H2-shaped hysteresis loop. This shaped hysteresis loop is usually found on mesoporous materials containing cylindrical-shaped channels with non-uniform pores. The pore size distribution curves (Figure 2b) were interpreted from the desorption branches of N_2 isotherm based on Barret-Joyner-Halenda (BJH) approach. Support and catalyst samples illustrated a pore size distribution smaller than 10 nm. The ZrO_2 support displayed the board peak centered at 6.0 nm of pore distribution with the surface area of 95 $m^2 \cdot g^{-1}$. The pore distribution was shifted downward the smaller pore size (4.0 nm) and a smaller surface area (75 $m^2 \cdot g^{-1}$) when the 10 wt.% Ni was impregnated onto the ZrO_2 support (the

10Ni/ZrO_2 catalyst). The downward shift is explained by the limitation of a specific surface area of ZrO_2 that decreases rapidly due to the blockage of pores by the large Ni particle size on the ZrO_2 support [19,21,35]. As is evident in Figure 2b, the Al_2O_3 support and the 10Ni-xZrO_2/Al_2O_3 (CI) catalysts possessed a narrower pore size distribution peak centered at approximately 2.4 to 2.7 nm. Because of the blocking effect, the co-impregnated 10 wt.% Ni-1 wt.% ZrO_2 and the 10 wt.% Ni-10 wt.% ZrO_2 onto the Al_2O_3 support decreased the surface area from 165 $m^2 \cdot g^{-1}$ to 153 $m^2 \cdot g^{-1}$ and 134 $m^2 \cdot g^{-1}$, respectively. Less surface area was detected from the 10Ni-10ZrO_2/Al_2O_3 (CI) by the reason of the large NiO particles from the low NiO dispersion in the catalyst for a high ZrO_2 content confirmed with Ni dispersion in the H_2-TPD results. Compared to the 10Ni-10ZrO_2/Al_2O_3 (CI) catalyst, the character of the surface area (112 $m^2 \cdot g^{-1}$) and the pore size distribution for the 10Ni-10ZrO_2/Al_2O_3 (SI) catalyst shifted toward the pore character of ZrO_2 support reflect the greater interaction of the ZrO_2-Al_2O_3.

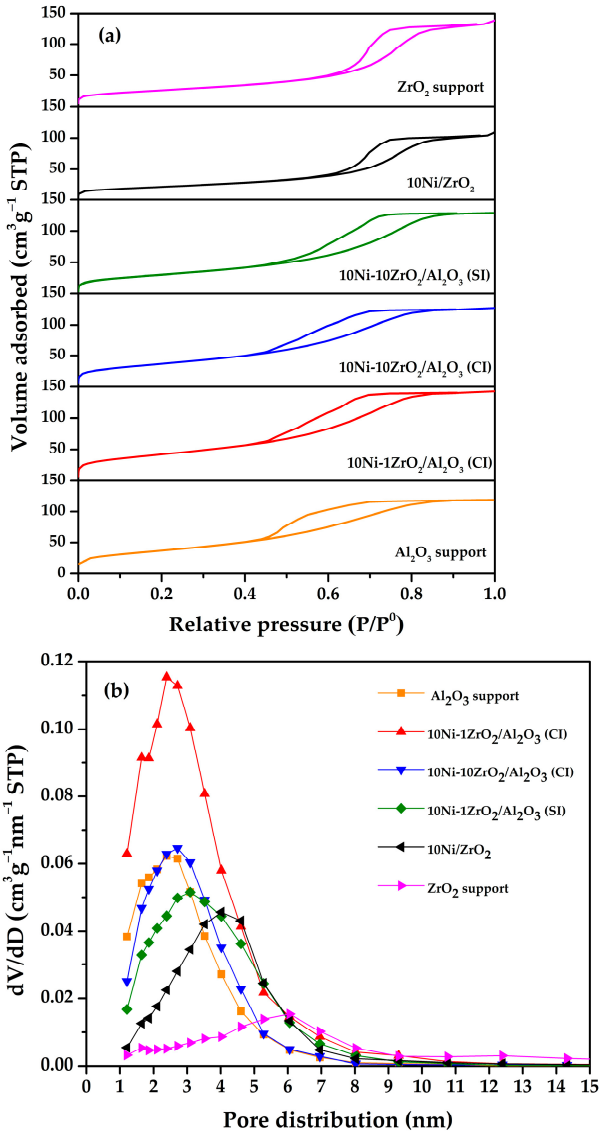

Figure 2. (**a**) N_2 adsorption-desorption isotherms and (**b**) BJH pore size distributions of Al_2O_3 support, ZrO_2 support, 10Ni/ZrO_2, 10Ni-1ZrO_2/Al_2O_3 (CI), 10Ni-10ZrO_2/Al_2O_3 (CI), and 10Ni-10ZrO_2/Al_2O_3 (SI).

2.3. H_2-Temperature Programmed Reduction

Three temperature ranges of reduction peaks were detected in the H_2-TPR profiles from 50 °C to 800 °C of all calcined catalysts (Figure 3). Peaks at low temperatures (350 °C to 500 °C) coincide with the reduction of isolated NiO at the catalyst surface as well as the reduction of NiO weakly interacting with the support [36]. The higher temperature peaks at approximately 500 °C to 650 °C are assigned to the reduction of NiO having a medium interaction with the support. Reduction peaks at temperatures over 650 °C reflect the reduction of the Ni^{2+} species in the strong metal-support interaction (SMSI) oxides (such as the $NiAl_2O_4$ spinel phases) [35,37]. The H_2-TPR profile of the 10Ni/ZrO_2 catalyst (ZrO_2 as support) displayed the peak shoulder centered at 425 °C and the large reduction peak centered at 545 °C. These overlapping peaks refer to the reduction of the NiO species in a weak and a medium interaction with the support [33]. The reduction at the low and medium temperatures with the greatest amount of H_2 consumption in the TPR profile of the 10Ni/ZrO_2 represents the reduction of large NiO particles with the weakest metal-support interaction among all samples. The reason could be ascribed to the low surface area of ZrO_2 support simultaneously with the poor NiO-ZrO_2 interaction. The H_2-TPR profiles of the different ZrO_2 contents on the surface of the 10Ni-xZrO_2/Al_2O_3 (CI) catalysts established two temperature peaks. The small peaks at low temperatures (centered at 405 °C to 410 °C) are correlated to the reduction of the NiO in the weak metal-support interaction [34]. The broad reduction peaks at 550 °C to 800 °C are attributed to the reduction of the Ni^{2+} species in a medium associated with a strong metal-support interaction [33,36,38]. The peak in H_2-TPR profile of 10Ni-10ZrO_2/Al_2O_3 (SI) starting at 550 °C indicates only the reduction of the NiO species in a medium and a strong metal-support interaction. When compared to 10Ni-10ZrO_2/Al_2O_3 (CI), peaks in the H_2-TPR profile of 10Ni-10ZrO_2/Al_2O_3 (SI) shifted toward higher temperatures. This characteristic corresponds to a stronger metal-support interaction representing the smaller and well-dispersed NiO species in 10Ni-10ZrO_2/Al_2O_3 (SI). Considering the result of the Ni dispersion, BJH pore distribution, and H_2-TPR that exhibited the stronger interaction in the 10Ni-10ZrO_2/Al_2O_3 (SI) catalyst, it suggests the formation of the ZrO_2-Al_2O_3 composite where the ZrO_2 probably incorporated into the Al_2O_3 at the first step of the sequential impregnation [35,39,40] before the Ni solution was loaded. The composite enhances the interaction between the Ni and the ZrO_2 in the ZrO_2-Al_2O_3 composite phase compared to the Ni and the ZrO_2 in the ZrO_2 phase.

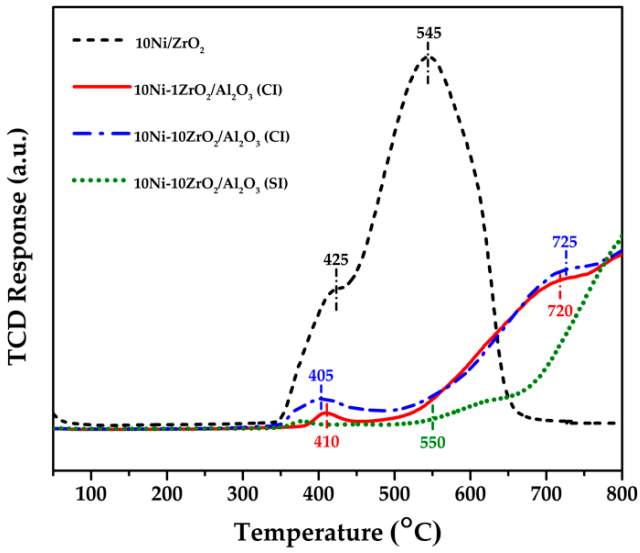

Figure 3. H_2-TPR profiles of all catalysts.

2.4. CO_2-Temperature Programmed Desorption

The basicity of the reduced catalyst relates to the catalytic ability of CO_2 adsorption and activation. Peaks as a function of temperature in CO_2-TPD profiles of reduced catalysts

(Figure 4) demonstrated the distribution of weak basic sites at 50 °C to 200 °C, moderate basic sites at 200 °C to 550 °C, and strong basic sites at temperature higher than 550 °C. The calculated number of basic sites in an individual type and in total are summarized in Table 2. Among all types of basic sites, the weak and moderate basic sites are crucial for CO_2 adsorption and activation without the effect of too strong adsorption. As informed in Table 2, the 10Ni/ZrO_2 catalyst possessed the lowest basicity while the 10Ni-1ZrO_2/Al_2O_3 (CI) catalyst displayed the highest number of the weak and moderate basic sites. The 10Ni-10ZrO_2/Al_2O_3 (CI) and 10Ni-10ZrO_2/Al_2O_3 (SI) catalysts presented a closing overall basic site. It implied that 10Ni-1ZrO_2/Al_2O_3 (CI) is the most active catalyst toward the CO_2 adsorption and activation in this work.

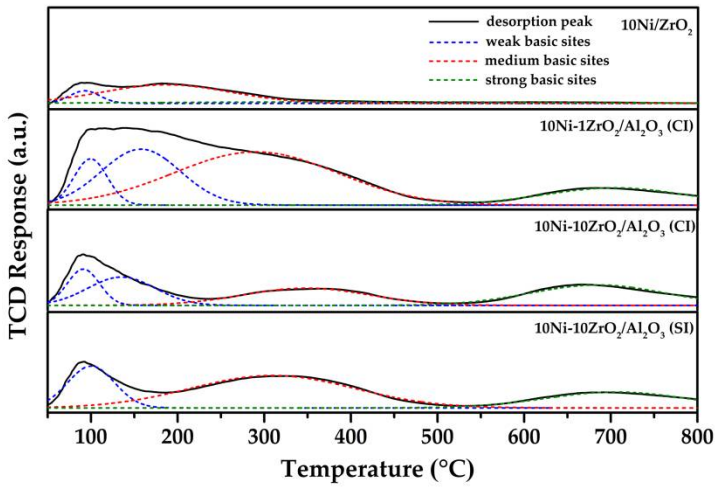

Figure 4. CO_2-TPD profiles of all catalysts.

Table 2. Deconvolution of the CO_2-TPD profiles and O_2-TPD profiles for all catalysts.

Samples	CO_2-TPD Deconvolution (mmol·g^{-1})				O_2-TPD Deconvolution (mmol·g^{-1})			
	Weak	Medium	Strong	Total Basicity	α Oxygen	β Oxygen	γ Oxygen	Total O_2 Desorption
10Ni/ZrO_2	0.058	0.042	0.007	0.107	0.151	0.020	0.005	0.176
10Ni-1ZrO_2/Al_2O_3 (CI)	0.191	0.225	0.034	0.450	0.009	0.260	0.028	0.297
10Ni-10ZrO_2/Al_2O_3 (CI)	0.081	0.046	0.047	0.174	0.008	0.215	0.121	0.344
10Ni-10ZrO_2/Al_2O_3 (SI)	0.069	0.112	0.030	0.211	0.017	0.316	0.096	0.429

2.5. O_2-Temperature Programmed Desorption

The oxygen mobility is a property of a catalyst that relates to its carbon resistance. In order to determine the oxygen mobility properties of reduced catalysts, O_2-TPD measurement was performed. O_2-TPD profiles (Figure 5) from 50 °C to 850 °C of all samples depicted three temperature ranges of desorption peaks. Peaks at low temperature (before 250 °C), known as α oxygen, are attributed to the desorption of weakly chemisorbed oxygen molecules on the surface. The peaks at 250 °C to 550 °C, known as β oxygen, are ascribed to the desorption of the oxygen species nearby the vacancy sites. Desorption peaks at temperature higher than 550 °C, known as γ oxygen, are assigned to the release of bulk lattice oxygen [41–43]. The total number of O_2 desorption of 10Ni/ZrO_2, 10Ni-1ZrO_2/Al_2O_3 (CI), 10Ni-10ZrO_2/Al_2O_3 (CI), and 10Ni-10ZrO_2/Al_2O_3 (SI) catalysts were 0.176, 0.297, 0.344, and 0.429 mmol·gcat^{-1} (Table 2), respectively. Although the O_2-TPD profile of the 10Ni/ZrO_2 catalyst (ZrO_2 as a support) demonstrated the minimum total O_2 desorption, it provided the highest numbers of α oxygen. When ZrO_2 located at the surface and interacted greater with Ni, the number of oxygen desorption increased with

the larger amounts of β and γ oxygen. It suggests more oxygen desorption from vacancy sites and the bulk lattice. Regarding to γ oxygen among 10Ni-1ZrO_2/Al_2O_3 (CI), 10Ni-10ZrO_2/Al_2O_3 (CI), and 10Ni-10ZrO_2/Al_2O_3 (SI) catalysts, the most uniform γ oxygen species was observed in the O_2-TPD profile of the 10Ni-10ZrO_2/Al_2O_3 (SI) catalyst. This result implies the most uniform NiO-ZrO_2 interaction in the bulk.

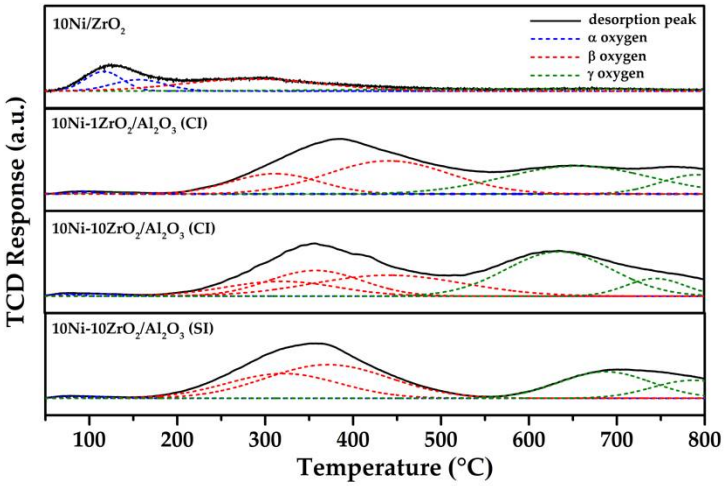

Figure 5. O_2-TPD profiles of profiles of all catalysts.

2.6. Catalytic Activity

The results of CRM catalytic tests over the Ni-based catalysts with the ZrO_2 as a different component are illustrated in Figure 6. Considering the CRM results with the characterization results, the 10Ni/ZrO_2 catalyst (ZrO_2 as a support) represented the lowest catalytic activity. This low activity is explained by its weakest Ni-ZrO_2 interaction compared to other catalysts, eventuating in the low dispersion with the large Ni particle size [44]. The similarly high CH_4 and CO_2 conversions were observed over the catalysts with a ZrO_2 promoter and a ZrO_2 coactive component. These relatively high catalytic activities are subjected to (i) the stronger interaction of the Ni-Al_2O_3 and/or the ZrO_2-Al_2O_3 composite in the 10Ni-xZrO_2/Al_2O_3 catalysts, leading to the better dispersion with the smaller Ni particle size that increases the Ni surface area [33,40] and (ii) the ZrO_2 surface that improves the CO_2 adsorption and dissociation. Furthermore, the reactant conversions of 10Ni-10ZrO_2/Al_2O_3 catalyst increased for 4% approximately after 200 min of time-on-stream. It can be hypothesized that after 200 min, the effective coke oxidation was involved in the CRM process due to the strongest metal-support interaction combined with the β oxygen species. The pathway of rapid oxygen transport from ZrO_2 through vacancies to Ni improves CO_2 activation-dissociation via vacancy sites of ZrO_2. This reason allowed CH_4 to be activated more efficiently on Ni. Figure 6c depicts that the H_2/CO ratio in the catalytic profile of all catalysts was lower than unity because of the reverse water-gas shift side reaction (R4). At the first 20 min of time-on-stream, H_2/CO ratio decreased for all the studied samples excluding 10Ni-1ZrO_2/Al_2O_3 (CI). It can be explained by the mechanism of CRM and CO_2-TPD results. Many studies reported that the CRM reaction involves CH_4 dissociation as well as CO_2 dissociation. The dissociative chemisorption of CH_4 was denoted as an initial step and other steps take place along the time. Because CH_4 is a source of H_2 and CO_2 can be counted as a source of CO in the syngas product, the decreasing trend of H_2/CO ratio of each catalyst was observed at the beginning. Differently, the stable lowest H_2/CO ratio was obtained from the 10Ni-1ZrO_2/Al_2O_3 (CI) catalyst as it is the most active catalyst material for CO_2 activation-dissociation (discussed in CO_2-TPD part) that can drive CO_2 dissociation since the beginning. Moreover, the H_2/CO ratio of 10Ni-10ZrO_2/Al_2O_3 (SI) was also low due to the high CO_2 activation-dissociation via the vacancies. In addition, the catalytic activities in this work are in the same range of literature data (Table 3).

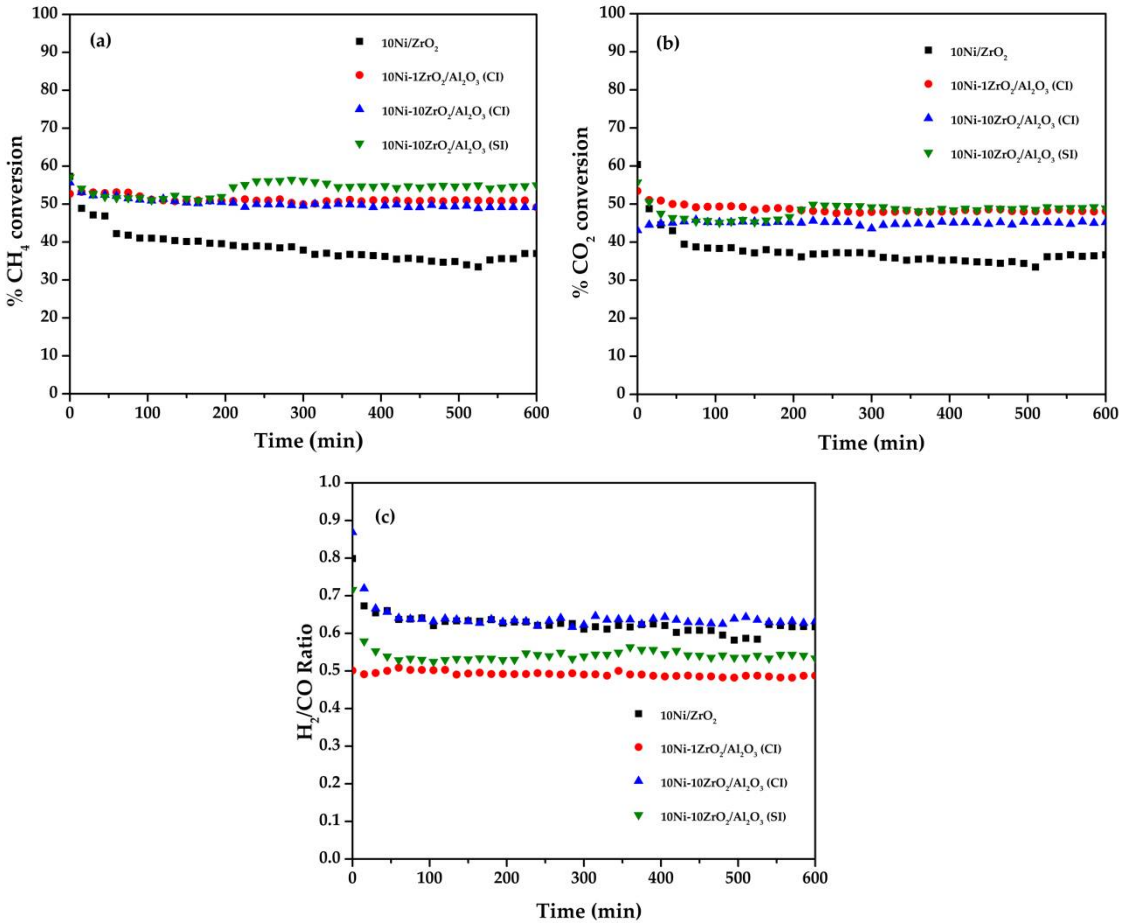

Figure 6. Results of CRM catalytic tests at 620 °C under ambient pressure: (**a**) CH_4 conversion, (**b**) CO_2 conversion, and (**c**) H_2/CO ratio.

Table 3. Comparison of the results of this work with those of literature.

Catalyst	Preparation Method	Reactor Type	Operating Temperature	% Conversion		Ref.
				CH_4	CO_2	
2.5%Ni nanosheet/ZrO_2	Wet impregnation	Fixed-bed quartz reactor	800 °C	46.0	60.0	[4]
10%Ni/m-ZrO_2-Al_2O_3	Evaporation-induced self-assembly	Fixed-bed quartz reactor	700 °C	60.2	78.0	[45]
15%Ni-7%ZrO_2/Al_2O_3	Sequential impregnation	Fixed-bed reactor	700 °C	42.5	n/a	[28]
3%Ni/ZrO_2 treated with N_2	Deposition-precipitation	Fixed-bed quartz microreactor	700 °C	62.5	63.0	[44]
10%Ni-10%ZrO_2/Al_2O_3	Sequential impregnation	Fixed-bed reactor	620 °C	54.3	49.8	This work

According to CRM results, the 10Ni-1ZrO_2/Al_2O_3 (CI) catalyst and the 10Ni-10ZrO_2/Al_2O_3 (SI) catalyst were more selective toward CO_2 activation-dissociation as a different behavior. Thus, these two catalysts were chosen here for investigation in a CSCRM test using a similar condition to CRM with the additional steam, and the results are shown in Figure 7. During the first 100 min of time-on-stream, the CH_4 conversion as well as the CO_2 conversion decreased to approximately constant, and the H_2/CO ratio became almost stable on both catalysts. It could be counted on the adjustment of such a complex reaction. After 100 min, the 10Ni-10ZrO_2/Al_2O_3 (SI) catalyst established lower CH_4 conversion, lower

CO_2 conversion, and higher H_2/CO ratio than those obtained from the 10Ni-1ZrO_2/Al_2O_3 (CI) catalyst. It implied that a larger number of active sites on the 10Ni-10ZrO_2/Al_2O_3 (SI) catalyst were occupied by the reaction loop of H_2O activation-dissociation compared to the 10Ni-10ZrO_2/Al_2O_3 (SI) catalyst. Consequently, the H_2O activation-dissociation was promoted greater on the basic sites than on the vacancy sites in CSCRM for this catalyst set.

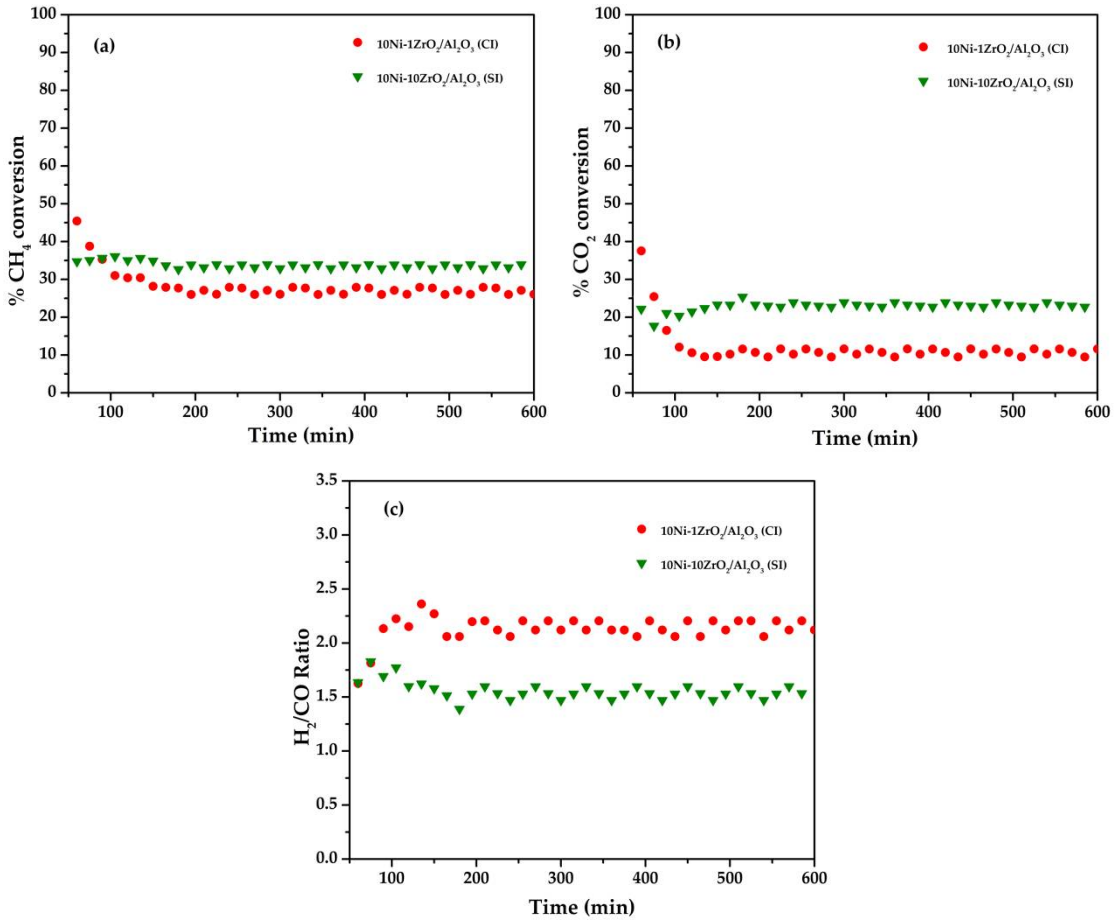

Figure 7. Results of CSCRM catalytic tests at 620 °C under ambient pressure: (**a**) CH_4 conversion, (**b**) CO_2 conversion, and (**c**) H_2/CO ratio.

2.7. Coke Deposition

The thermogravimetric analysis (TGA) and the derivative thermogravimetric (DTG) curves of spent catalysts (Figure 8) were employed to evaluate the carbon deposition over the catalyst during the CRM tests. The weight loss in the TGA curve reflects the amount of deposited coke and the temperature at which different types of coke are oxidized, indicating the difficulty of their removal. The TGA/DTG profile of the spent 10Ni/ZrO_2 catalyst (Figure 8a) represented two temperature ranges for a total weight loss of 22% relating to the oxidation of the graphitic carbon (350 °C to 550 °C) and the filament carbon (550 °C to 700 °C) [16,46,47]. The high quantity of carbon formation was observed on the spent 10Ni/ZrO_2 catalyst according to the low dispersion of large Ni on the catalyst surface because of the poor Ni-ZrO_2 interaction as found in the H_2-TPD results and the lowest number of oxygen desorption as discussed in the O_2-TPD results. The weight loss of 17% and 32% was monitored in the TGA/DTG profiles of the spent 10Ni-1ZrO_2/Al_2O_3 (CI) catalyst (Figure 8b) and the spent 10Ni-10ZrO_2/Al_2O_3 (CI) catalyst (Figure 8c), respectively. The coke combustion occurred in the similar range of 550 °C to 800 °C corresponding to the oxidation of the filament/graphitic carbon species [48], the main type of the catalyst deactivation growing on the poor Ni-ZrO_2 interaction. Although the catalysts prepared by

the co-impregnation exhibited the similar oxygen mobility and type of coke, the amount of coke on a catalyst with a low content of ZrO_2 at the surface as promoter (the 10Ni-1ZrO_2/Al_2O_3 (CI) catalyst) is less than the coke on the catalyst with a high content of ZrO_2 at the surface as a coactive species (the 10Ni-10ZrO_2/Al_2O_3 (CI) catalyst). Thereby, the carbon deposition amount reduced with a decrease of the ZrO_2 content due to the lower effect of a poor Ni-ZrO_2 interaction providing to the smaller Ni particle sizes. Moreover, compared to the spent 10Ni-10ZrO_2/Al_2O_3 (CI) catalyst, the coke proportion on the spent 10Ni/ZrO_2 catalyst was lower. It can be ascribed to the desorption of α oxygen on the 10Ni/ZrO_2 catalyst, which practically eliminates the amount of deposited coke and inhibits filament carbon. Finally, the continuous weight loss of 7% appeared mostly at a temperature below 300 °C on the spent 10Ni-10ZrO_2/Al_2O_3 (SI) (ZrO_2 as a coactive component) catalyst (Figure 8d), correlating to the oxidation of the amorphous carbon. The deposited coke on the spent 10Ni-10ZrO_2/Al_2O_3 (SI) catalyst was found not only in the lesser amount but also in an easier removal characteristic compared to other catalysts. Considering the O_2-TPD and the H_2-TPR results, the reason for this easier removal is attributed to the high amount of oxygen mobility accompanied with the greater interaction between Ni and the ZrO_2-Al_2O_3 composite that enhances both the Ni distribution (resulting in smallest Ni particle sizes) and pathway of the vacancy sites for the oxygen transfer from ZrO_2 in ZrO_2-Al_2O_3 through coke on the Ni surface in the CRM process [27,28,49].

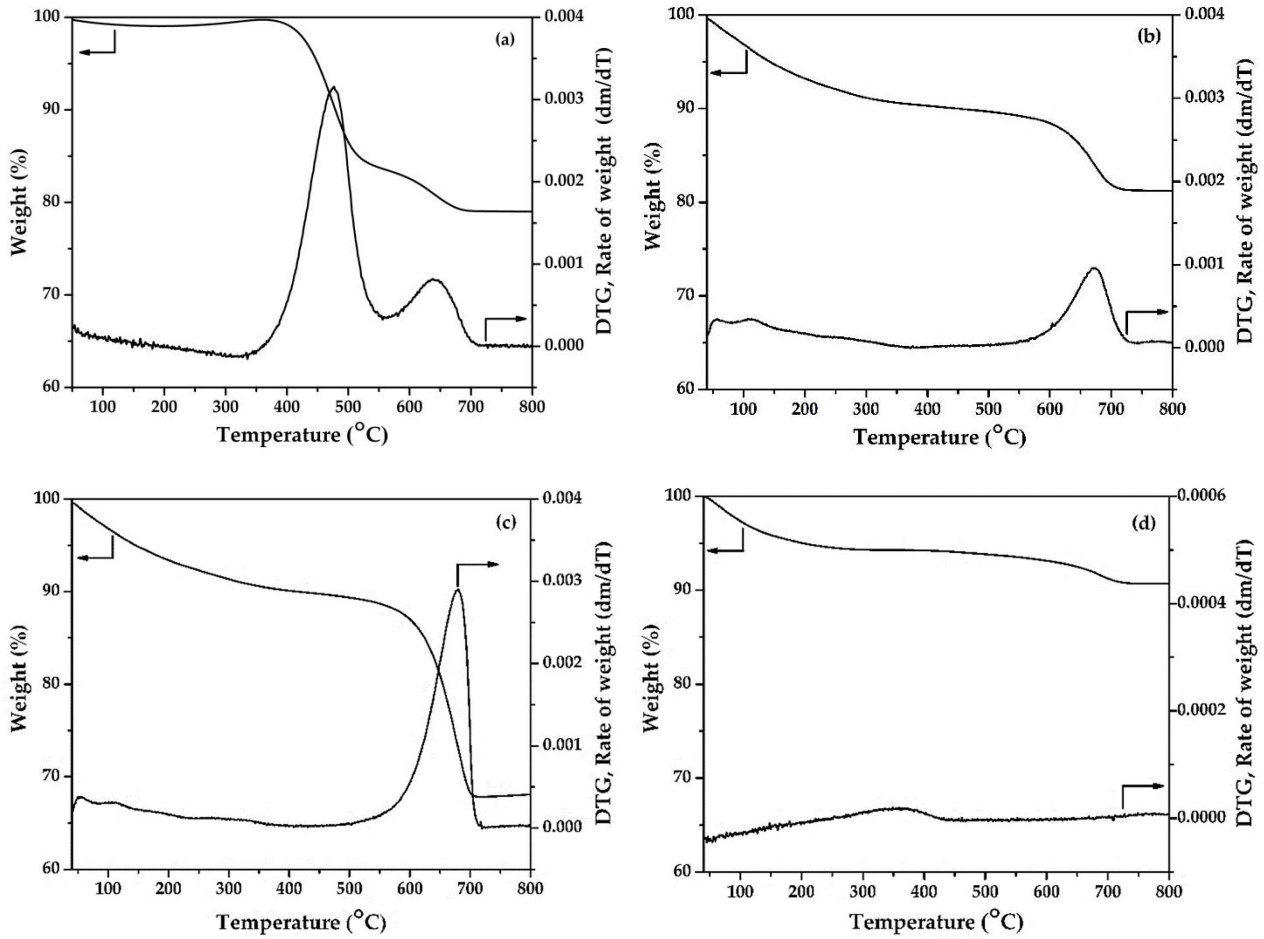

Figure 8. TGA/DTG profiles of the spent (**a**) 10Ni/ZrO_2, (**b**) 10Ni-1ZrO_2/Al_2O_3 (CI), (**c**) 10Ni-10ZrO_2/Al_2O_3 (CI), and (**d**) 10Ni-10ZrO_2/Al_2O_3 (SI).

The coke deposition on the spent catalysts of CSCRM was determined by TPO results (Figure 9). In the TPO profiles of the carbon deposition on the spent 10Ni-1ZrO_2/Al_2O_3 (CI) catalyst and 10Ni-10ZrO_2/Al_2O_3 (SI) catalysts used in CSCRM, two peaks of carbon

removal depended on the carbon types were observed. Peaks at low temperature (50 °C to 350 °C) and peaks at high temperature (500 °C to 750 °C) in the profiles correlate to the amorphous carbon and the filament carbon, respectively. The quantity of carbon deposition over the spent catalysts was calculated directly from the peak area. As a result, the coke formation appeared mostly as the filament carbon. The total amount of coke on the spent 10Ni-1ZrO_2/Al_2O_3 (CI) and the spent 10Ni-10ZrO_2/Al_2O_3 (SI) from CSCRM were 1.213 mmol·g^{-1} and 1.571 mmol·g^{-1}, respectively. For comparison purpose, in CSCRM process, the coke resistance/removal of 10Ni-1ZrO_2/Al_2O_3 (CI) is more effective than those of the 10Ni-10ZrO_2/Al_2O_3 (SI). It can be ascribed to more oxygen surface from H_2O activation-dissociation promoted via weak and moderate basic sites on the catalyst [50].

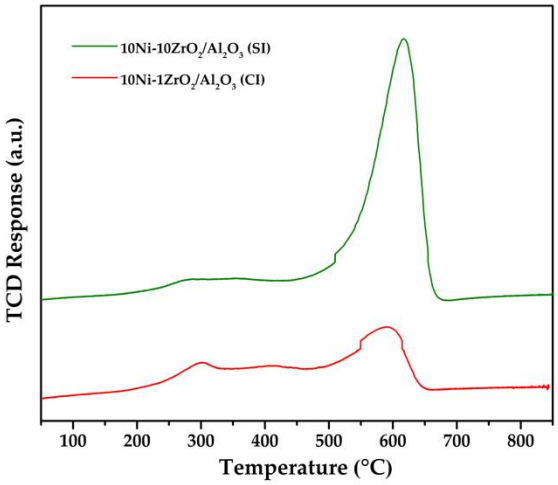

Figure 9. TPO profiles of profiles of the spent catalysts after the CSCRM reaction.

3. Materials and Methods

3.1. Catalyst Preparation

The ZrO_2 support was synthesized via the precipitation method. The solution 0.4 M zirconyl chloride ($ZrOCl_2$, Sigma Aldrich, St. Louis, MS, USA) was used as a precursor, and a 2 M ammonium hydroxide (NH_4OH, 65% PanReac AppliChem ITW Reagents) solution was used as a precipitant. These two aqueous solutions were added by drops into a beaker with a controlled pH of 9.3. Then, the mixture was stirred thoroughly for 30 min at 60 °C, and the precipitate was aged overnight at the ambient temperature. The precipitate powder was vacuum filtered out and rinsed with distilled water until neutral (with a pH of approximately 7). Afterwards, it was dried overnight at 70 °C and calcined in the air at 750 °C for 5 h. The 10 wt.% Ni/ZrO_2 catalyst was prepared by impregnating it with a 10 wt.% of nickel (II) nitrate hexahydrate solution ($Ni(NO_3)_2{\cdot}6H_2O$, 98%, Acros OrganicsTM) onto the ZrO_2 support followed by drying at 50 °C overnight and calcination in the air at 650 °C for 6 h.

The Al_2O_3 support was synthesized by the sol–gel method using aluminium isopropoxide ($C_9H_{21}AlO_3$, 98%, Acros OrganicsTM) and nitric acid (65% CARLO ERBA Reagents) as precursors. The gel product was dried at 50 °C overnight and calcined at 650 °C for 6 h with a heating rate of 3 °C min^{-1}. The 10 wt.% Ni-x wt.% ZrO_2/Al_2O_3 catalysts (denoted as 10Ni-xZrO_2/Al_2O_3 (CI); x = 1 and 10) were prepared by co-impregnation method. The aqueous solution of the desired amount of zirconium (IV) oxynitrate hydrate ($ZrO(NO_3)_2{\cdot}H_2O$, Sigma Aldrich) mixed with $Ni(NO_3)_2{\cdot}6H_2O$ was added dropwise to the Al_2O_3 support. The resulting wet powder was followed by drying and calcination using the same conditions used for the 10Ni/ZrO_2 catalyst. To generate the different interactions of Ni-ZrO_2, the sequential impregnation (SI) method was employed to prepare the 10 wt.% Ni-10 wt.% ZrO_2/Al_2O_3 catalyst (denoted as 10Ni-10Zr/Al_2O_3(SI)). First, Al_2O_3 support was impregnated with an aqueous solution of zirconium (IV) oxynitrate hydrate followed by drying and calcination, using the condition for 10Ni-xZr/Al_2O_3 (CI). Second, 10 wt.%

ZrO_2/Al_2O_3 was impregnated with a $Ni(NO_3)_2 \cdot 6H_2O$ solution followed by drying and calcination, using similar condition as with $10Ni/ZrO_2$.

3.2. Catalysts Characterization

The X-ray diffraction (XRD) patterns of the reduced catalysts were collected on a Bruker AXS Model D8-Discover (Bruker AXS, Billerica, MA, USA) with a Cu Kα radiation (λ = 0.154 nm), operating at 40 kV and 40 mA and with a scanning range between 20° to 70° with a step width of a scanning speed of 0.02° min^{-1}.

The metal particle size (d, nm) and the metal dispersion (D_m, %) were indirectly determined by the hydrogen temperature desorption (H_2-TPD) technique performed in a BELCAT-basic system (BEL JAPAN, INC., Osaka, Japan). At the beginning, the catalyst (0.05 g) was preactivated at 600 °C in pure H_2 flow for 2 h, followed by cooling to 100 °C in He flow. Then, the catalyst was isothermally chemisorbed on the surface with pure H_2 at 100 °C for 1 h and cooled to 40 °C in He flow. The quantity of H_2 desorbed was measured by passing He flow through the catalyst from 50 °C to 850 °C at the rate of 10 °C min^{-1}. The metal particle size (Equation (1)) and the metal dispersion (Equation (2)) were calculated based on the stoichiometry of the hydrogen monolayer chemisorption uptake.

$$\%D_m = \frac{\left(\frac{V_{chem}}{22{,}414}\right) \times SF \times MW}{\left(\frac{m \times w}{100}\right)} \times 100 \quad (1)$$

$$d = \frac{6000}{\frac{\left(\frac{V_{chem}}{22{,}414}\right) \times SF \times 6.02 \times 10^{23} \times \rho \times \sigma_m \times 10^{-18}}{\left(\frac{m \times w}{100}\right)}} \quad (2)$$

where V_{chem} is the amount of desorbed hydrogen (cm^3), SF is a stoichiometry factor (Ni mol:H_2 mol in the H_2 chemisorption = 2), MW is an atomic weight of metal (g mol^{-1}), m is a sample weight (g), w is a wt.% of supported metal content, σ_m is a cross-sectional area of one Ni atom (the area occupied by Ni atom = 0.0649 nm^2), and ρ is a density of metal (g cm^{-3}).

The surface area and pore properties of the catalysts were determined using the N_2 adsorption–desorption isotherm at the boiling temperature of liquid N_2 (−196 °C) on a BELSORP-mini II. Prior (BEL JAPAN, INC., Osaka, Japan). Prior to the experiment, the catalyst was degassed at 350 °C under a N_2 flow for 4 h. The surface area and the pore volume were evaluated by the Brunauer–Emmett–Teller (BET) analysis method. The pore size distribution was calculated based on the Barett–Joyner–Halenda (BJH) method.

The reducibility of the catalysts was measured by the temperature-programmed reduction in hydrogen (H_2-TPR) employing a BELCAT-basic system (BEL JAPAN, INC., Osaka, Japan) equipped with a thermal conductivity detector (TCD). Prior to measurement, a 0.05 g catalyst was degassed at 220 °C for 1 h and cooled to 40°C in Ar. Then, the sample was reduced in a 5 vol.% H_2/Ar flow (30 mL min^{-1}) from 50 °C to 800 °C at the ramping rate of 10 °C min^{-1}.

The basicity of the reduced catalysts was characterized by the temperature-programmed desorption in carbon dioxide (CO_2-TPD) using a BELCAT-basic system apparatus (BEL JAPAN, INC., Osaka, Japan) apparatus. Prior to the TPD experiment, the catalyst (0.05 g) was pre-treated by heating at 220 °C for 1 h in He. Then, the catalyst was cooled to 40°C under He flow and reduced in situ at 620°C for 2 h with pure H_2 flow (30 mL min^{-1}) followed by cooling to 40°C in He flow. Subsequently, adsorption of CO_2 was performed in pure CO_2 flow (30 mL min^{-1}) at 40°C for 1 h. The physisorbed CO_2 was removed with He flow. Afterward, the sample was heated from 50 °C to 850 °C at a rate of 10 °C min^{-1} in He flow, and the desorbed CO_2 was detected.

The oxygen mobility of the catalysts was evaluated by the temperature-programmed desorption in oxygen (O_2-TPD) on a BELCAT-basic system (BEL JAPAN, INC., Osaka, Japan). Before the O_2-TPD testing, the 0.05 g catalyst was reduced in-situ at 600 °C in a pure H_2 flow for 1.5 h and cooled to 200 °C in flowing Ar. Afterward, a pure O_2 gas was introduced to be adsorbed on the catalyst surface at 200 °C for 1.5 h. Then, the catalyst was

purged in Ar flow to flush weakly adsorbed O_2 on the surface. After purging, the catalyst was heated from 50 °C to 850 °C in Ar flow (30 mL min^{-1}) at the constant ramping rate of 10 °C min^{-1}. The desorbed O_2 was monitored by TCD.

The quantity and types of deposited carbon over the spent catalysts from the CRM test were investigated by the mean of the thermogravimetric analysis (TGA) on a METTLER TOLEDO thermogravimetric analyzer (METTLER TOLEDO, Columbus, OH, USA). A 0.012 g sample of spent catalyst was combusted in an air stream from 40 °C to 800 °C at a heating rate of 10 °C min^{-1}.

The amount and types of the coke accumulated on the spent catalysts during the CSCRM test reaction were interpreted by temperature-programmed oxidation (TPO) via a BELCAT-basic system (BEL JAPAN, INC., Osaka, Japan). Before the TPO measurement, in Ar flow (30 mL min^{-1}), a 0.050 g of the spent catalyst was pretreated at 220 °C for 2 h followed by cooling to 40 °C. Afterwards, the spent catalyst was oxidized in a 5 vol.% O_2/Ar flow (30 mL min^{-1}) with a ramping rate of 10 °C min^{-1} from 50 °C to 800 °C and the O_2 consumption was detected.

3.3. Catalytic Tests

The CRM reaction was performed in a tubular fixed-bed reactor at 620 °C for 10 h. Before the test, the catalyst (0.200 g) was in situ reduced in a pure H_2 (purity 99.999%) at 620 °C for 6 h. Then, the feed molar composition of $CH_4/CO_2/N_2$ = 3/5/4 at a total flow rate of 60 mL min^{-1} was introduced to the reactor. The outlet gas was analyzed via on-line gas chromatograph (Agilent GC7890A Agilent, Santa Clara, CA, USA) equipped with the TCD. The CSCRM reaction was conducted for 6 h using the same system and operating conditions of CRM with the additional steam (the CH_4:CO_2:H_2O:N_2 ratio of 3:5:2.4:4 with overall flow rate of 72 mL min^{-1}). The catalyst performance was evaluated in terms of a CH_4 conversion (Equation (3)), CO_2 conversion (Equation (4)) and H_2/CO ratio (Equation (5)) as expressed in the following equations:

$$X_{CH_4}(\%) = \frac{(CH_4)_{in} - (CH_4)_{out}}{(CH_4)_{in}} \times 100 \quad (3)$$

$$X_{CO_2}(\%) = \frac{(CO_2)_{in} - (CO_2)_{out}}{(CO_2)_{in}} \times 100 \quad (4)$$

$$H_2/CO \text{ ratio} = \frac{(H_2)_{out}}{(CO)_{out}} \quad (5)$$

4. Conclusions

This research is an in-depth examination of the role of ZrO_2 as various components in the Ni-based catalysts for CRM. The 10 wt.% Ni/ZrO_2 catalyst (10Ni/ZrO_2) was prepared by the impregnation method. The 10 wt.% Ni/Al_2O_3 catalyst with a 1 wt.% ZrO_2 promoter was prepared by the co-impregnation method (10Ni-1Zr/Al_2O_3(CI)). The 10 wt.% Ni/Al_2O_3 catalysts with a 10 wt.% ZrO_2 coactive component were prepared by the co-impregnation (10Ni-10Zr/Al_2O_3(CI)) and sequential impregnation methods (10Ni-10Zr/Al_2O_3(SI)) in order to study the effect of the different interactions in the catalyst. All catalysts were characterized and tested for CRM at 620°C under atmospheric pressure. The influence of ZrO_2 on the catalytic activity and the coke resistance mainly relies on the ZrO_2 content, Ni-ZrO_2 interaction, basicity, and oxygen mobility of catalysts. The lowest H_2/CO ratio (highest CO selectivity) were obtained from 10Ni-1Zr/Al_2O_3(CI) due to the weak and medium basic sites that promote the CO_2 activation-dissociation. Normally, ZrO_2 has a poor interaction with Ni that causes the low Ni dispersion with the large Ni particle sizes. Therefore, the 10Ni/ZrO_2 catalyst exhibited the lowest activity (CH_4 conversion of 40% and CO_2 conversion of 39%) due to the large Ni particle sizes from the Ni-ZrO_2 poor interaction. Because of the smallest number of total oxygen mobility, the relatively high amount of carbon (the weight loss of 22% in TGA curve of the spent catalyst) was

detected on this catalyst. The 10 wt.% Ni/Al_2O_3 catalysts with the lesser proportion of ZrO_2 (10Ni-1Zr/Al_2O_3(CI) and 10Ni-10Zr/Al_2O_3(CI)) illustrated the greater Ni dispersion resulting in higher activity (CH_4 conversion of 51% to 54% and CO_2 conversion of 45% to 50%). Although all catalysts provided the similar number of oxygen mobility. The high activity with a most practical carbon resistance (the weight loss of 7%in TGA curve of the spent catalyst) was successfully developed in 10Ni-10Zr/Al_2O_3(SI). The reason is explained by the great amount of oxygen mobility associated with the intimate interaction of the Ni and ZrO_2-Al_2O_3 composite in this catalyst enlarges the transferring oxygen from ZrO_2 to Ni, which increases the oxidation of carbon on the Ni surface via vacancies.

According to the basicity and oxygen mobility effect from CRM results, CSCRM at the similar condition of CRM with the addition of steam was performed on the 10Ni-1Zr/Al_2O_3(CI) catalyst and the 10Ni-10Zr/Al_2O_3(SI) catalyst. The higher H_2/CO ratio (2.1) with the lower carbon deposition (1.213 $mmol \cdot g^{-1}$) was monitored on the 10Ni-1Zr/Al_2O_3(CI) catalyst. It demonstrated that the basic sites enhance the H_2O activation-dissociation greater than the oxygen vacancy. However, this catalytic behavior causes a loss of active sites for CH_4 activation-dissociation. Overall, the results of our study offer useful information for the further Ni-based catalyst development.

Author Contributions: Conceptualization, W.S. and M.P. Data curation, W.S. and M.P. Investigation, W.S., S.S. and M.P. Methodology, W.S. and M.P. Formal analysis, W.S. and M.P. Funding support, S.S. and M.P. Writing—original draft, W.S. and M.P. Writing—review and editing, W.S., S.S. and M.P. Supervision, M.P. All authors have read and agreed to the published version of the manuscript.

Funding: The authors gratefully acknowledge the research grant from Faculty of Applied Science, King Mongkut's University of Technology North Bangkok (grant number. 6341106) and Thailand Graduate Institute of Science and Technology (TGIST) (grant number. SCA-CO-2563-12079-TH).

Data Availability Statement: Data sharing not applicable.

Conflicts of Interest: The authors declared no potential conflict of interest with respect to the research, authorship, and/or publication of this article.

References

1. Shamskar, F.R.; Rezaei, M.; Meshkani, F. The influence of Ni loading on the activity and coke formation of ultrasound-assisted co-precipitated Ni–Al_2O_3 nanocatalyst in dry reforming of methane. *Int. J. Hydrogen Energy* **2017**, *42*, 4155–4164. [CrossRef]
2. Şener, A.N.; Günay, M.E.; Leba, A.; Yıldırım, R. Statistical review of dry reforming of methane literature using decision tree and artificial neural network analysis. *Catal. Today* **2018**, *299*, 289–302. [CrossRef]
3. Kong, W.; Fu, Y.; Guan, C.; Pan, B.; Yuan, C.; Li, S.; Cai, F.; Zhang, J.; Sun, Y. Facile Synthesis of Highly Coking-Resistant and Active Nickel-Based Catalyst for Low-Temperature CO_2 Reforming of Methane. *Energy Technol.* **2019**, *7*, 1–11. [CrossRef]
4. Tathod, A.P.; Hayek, N.; Shpasser, D.; Simakov, D.S.A.; Gazit, O.M. Mediating interaction strength between nickel and zirconia using a mixed oxide nanosheets interlayer for methane dry reforming. *Appl. Catal. B Environ.* **2019**, *249*, 106–115. [CrossRef]
5. Abdulrasheed, A.; Jalil, A.A.; Gambo, Y.; Ibrahim, M.; Hambali, H.U.; Hamid, M.Y.S. A review on catalyst development for dry reforming of methane to syngas: Recent advances. *Renew. Sustain. Energy Rev.* **2019**, *108*, 175–193. [CrossRef]
6. Niu, J.; Liland, S.E.; Yang, J.; Rout, K.R.; Ran, J.; Chen, D. Effect of oxide additives on the hydrotalcite derived Ni catalysts for CO2 reforming of methane. *Chem. Eng. J.* **2019**, *377*, 119763. [CrossRef]
7. Olah, G.A.; Goeppert, A.; Czaun, M.; Mathew, T.; May, R.B.; Prakash, G.K.S. Single Step Bi-reforming and Oxidative Bi-reforming of Methane (Natural Gas) with Steam and Carbon Dioxide to Metgas (CO-$2H_2$) for Methanol Synthesis: Self-Sufficient Effective and Exclusive Oxygenation of Methane to Methanol with Oxygen. *J. Am. Chem. Soc.* **2015**, *137*, 8720–8729. [CrossRef] [PubMed]
8. Stroud, T. Chemical CO_2 recycling via dry and bi reforming of methane using Ni-Sn/Al_2O_3 and Ni-Sn/CeO_2-Al_2O_3 catalysts. *Appl. Catal. B Environ.* **2017**, *224*, 125–135. [CrossRef]
9. Tillmann, L.; Schulwitz, J.; Van Veen, A.; Muhler, M. Dry Reforming of Methane at High Pressure in a Fixed-Bed Reactor with Axial Temperature Profile Determination. *Catal. Lett.* **2018**, *148*, 2256–2262. [CrossRef]
10. Arbag, H.; Tasdemir, H.M.; Yagizatli, Y.; Kucuker, M.; Yasyerli, S. Effect of Preparation Technique on the Performance of Ni and Ce Incorporated Modified Alumina Catalysts in CO_2 Reforming of Methane. *Catal. Lett.* **2020**, *150*, 3256–3268. [CrossRef]
11. Jang, W.J. Combined steam and carbon dioxide reforming of methane and side reactions: Thermodynamic equilibrium analysis and experimental application. *Appl. Energy.* **2016**, *173*, 80–91. [CrossRef]
12. Whang, H.S.; Lim, J.; Choi, M.S.; Lee, J.; Lee, H. Heterogeneous catalysts for catalytic CO_2 conversion into value-added chemicals. *BMC Chem. Eng.* **2019**, *1*, 9. [CrossRef]

13. Kumar, N.; Shojaee, M.; Spivey, J.J. Catalytic bi-reforming of methane: From greenhouse gases to syngas. *Curr. Opin. Chem. Eng.* **2015**, *9*, 8–15. [CrossRef]
14. Batebi, D.; Abedini, R.; Mosayebi, A. Combined steam and CO_2 reforming of methane (CSCRM) over Ni–Pd/Al_2O_3 catalyst for syngas formation. *Int. J. Hydrogen Energy* **2020**, *45*, 14293–14310. [CrossRef]
15. Sangsong, S.; Ratana, T.; Tungkamani, S.; Sornchamni, T.; Phongaksorn, M.; Croiset, E. The Demonstration of the Superiority of the Dual Ni-Based Catalytic System for the Adjustment of the H_2/CO Ratio in Syngas for Green Fuel Technologies. *Catalysts* **2020**, *10*, 1056. [CrossRef]
16. Zhao, Z.; Ren, P.; Li, W.; Miao, B. Effect of mineralizers for preparing ZrO_2 support on the supported Ni catalyst for steam-CO_2 bi-reforming of methane. *Int. J. Hydrogen Energy* **2017**, *42*, 6598–6609. [CrossRef]
17. Chawl, S.K.; George, M.; Patel, F.; Patel, S. Production of Synthesis Gas by Carbon Dioxide Reforming of Methane over Nickel based and Perovskite Catalysts. *Procedia Eng.* **2013**, *51*, 461–466. [CrossRef]
18. Charisiou, N.; Papageridis, K.; Siakavelas, G.; Sebastian, V.; Hinder, S.; Baker, M.; Polychronopoulou, K.; Goula, M. The influence of SiO_2 doping on the Ni/ZrO_2 supported catalyst for hydrogen production through the glycerol steam reforming reaction. *Catal. Today* **2019**, *319*, 206–219. [CrossRef]
19. Li, Z.; Liu, C.; Zhang, X.; Wang, W.; Wang, B.; Ma, X. Effect of ZrO_2 on Catalyst Structure and Catalytic Sulfur-Resistant Methanation Performance of MoO_3/ZrO_2–Al_2O_3 Catalysts. *Kinet. Catal.* **2018**, *59*, 481–488. [CrossRef]
20. Cai, M.; Wen, J.; Chu, W.; Cheng, X.; Li, Z. Methanation of carbon dioxide on Ni/ZrO_2-Al_2O_3 catalysts: Effects of ZrO_2 promoter and preparation method of novel ZrO_2-Al_2O_3 carrier. *J. Nat. Gas Chem.* **2011**, *20*, 318–324. [CrossRef]
21. Guo, C.; Wu, Y.; Qin, H.; Zhang, J. CO methanation over ZrO_2/Al_2O_3 supported Ni catalysts: A comprehensive study. *Fuel Process. Technol.* **2014**, *124*, 61–69. [CrossRef]
22. Liu, Q.; Gu, F.; Gao, J.; Li, H.; Xu, G.; Su, F. Coking-resistant Ni-ZrO_2/Al_2O_3 catalyst for CO methanation. *J. Energy Chem.* **2014**, *23*, 761–770. [CrossRef]
23. Therdthianwong, S.; Siangchin, C.; Therdthianwong, A. Improvement of coke resistance of Ni/Al_2O_3 catalyst in CH_4/CO_2 reforming by ZrO_2 addition. *Fuel Process. Technol.* **2008**, *89*, 160–168. [CrossRef]
24. Calles, J.A.; Carrero, A.; Vizcaíno, A.J.; Lindo, M. Effect of Ce and Zr Addition to Ni/SiO_2 Catalysts for Hydrogen Production through Ethanol Steam Reforming. *Catalysts* **2015**, *5*, 58–76. [CrossRef]
25. Barroso-Quiroga, M.M.; Castro-Luna, A.E. Catalytic activity and effect of modifiers on Ni-based catalysts for the dry reforming of methane. *Int. J. Hydrogen Energy* **2010**, *35*, 6052–6056. [CrossRef]
26. Fakeeha, A. Hydrogen production by partial oxidation reforming of methane over ni catalysts supported on high and low surface area Alumina and Zirconia. *Processes* **2020**, *8*, 499. [CrossRef]
27. Lou, Y.; Steib, M.; Zhang, Q.; Tiefenbacher, K.; Horváth, A.; Jentys, A.; Liu, Y.; Lercher, J.A. Design of stable Ni/ZrO_2 catalysts for dry reforming of methane. *J. Catal.* **2017**, *356*, 147–156. [CrossRef]
28. Therdthianwong, S.; Therdthianwong, A.; Siangchin, C.; Yongprapat, S. Synthesis gas production from dry reforming of methane over Ni/Al_2O_3 stabilized by ZrO_2. *Int. J. Hydrogen Energy* **2008**, *33*, 991–999. [CrossRef]
29. Seo, J.G.; Youn, M.H.; Cho, K.M.; Park, S.; Lee, S.H.; Lee, J.; Song, I.K. Effect of Al_2O_3-ZrO_2 xerogel support on hydrogen production by steam reforming of LNG over Ni/Al_2O_3-ZrO_2 catalyst. *Korean J. Chem. Eng.* **2008**, *25*, 41–45. [CrossRef]
30. Roh, H.S.; Koo, K.Y.; Joshi, U.D.; Yoon, W.L. Combined H_2O and CO_2 reforming of methane over Ni-Ce-ZrO_2 catalysts for gas to liquids (GTL). *Catal. Lett.* **2008**, *125*, 283–288. [CrossRef]
31. Iglesias, I.; Forti, M.; Baronetti, G.; Mariño, F. Zr-enhanced stability of ceria based supports for methane steam reforming at severe reaction conditions. *Int. J. Hydrogen Energy* **2019**, *44*, 8121–8132. [CrossRef]
32. Weckhuysen, B.M.; Wachs, I.E. Catalysis by supported metal oxides. In *Handbook of Surfaces and Interfaces of Materials*; Academic Press: San Diego, CA, USA, 2001; Volume 1, pp. 613–648.
33. Lanre, M.S.; Al-Fatesh, A.S.; Fakeeha, A.H.; Kasim, S.O.; Ibrahim, A.A.; Al-Awadi, A.S.; Al-Zahrani, A.A.; Abasaeed, A.E. Catalytic Performance of Lanthanum Promoted Ni/ZrO_2 for Carbon Dioxide Reforming of Methane. *Processes* **2020**, *8*, 1502. [CrossRef]
34. Fakeeha, A.H.; Arafat, Y.; Ibrahim, A.A.; Shaikh, H.; Atia, H.; Abasaeed, A.E.; Armbruster, U.; Al-Fatesh, A.S. Highly Selective Syngas/H_2 Production via Partial Oxidation of CH_4 Using (Ni, Co and Ni–Co)/Zr–Al_2O_3 Catalysts: Influence of Calcination Temperature. *Processes* **2019**, *7*, 141. [CrossRef]
35. Gandhi, S.P.; Patel, S. Dry Reforming of Methane over Supported Nickel Catalysts Promoted by Zerconia, Ceria and Magnesia. *Int. J. Adv. Res. Eng. Technol.* **2015**, *6*, 131–146.
36. Santos, D.C.R.M.; Lisboa, J.S.; Passos, F.B.; Noronha, F.B. Characterization of steam-reforming catalysts. *Braz. J. Chem. Eng.* **2004**, *21*, 203–209. [CrossRef]
37. Sajjadi, S.M.; Haghighi, M.; Rahmani, F. Sol-gel synthesis and catalytic performance of Ni-Co/Al_2O_3-MgO-ZrO_2 nanocatalyst with different ZrO_2-loadings used in CH_4/CO_2 reforming for hydrogen production. *Int. J. Oil Gas Coal Technol.* **2014**, *8*, 304–324. [CrossRef]
38. Zhou, L.; Li, L.; Wei, N.; Li, J.; Basset, J.-M. Effect of $NiAl_2O_4$ Formation on Ni/Al_2O_3 Stability during Dry Reforming of Methane. *ChemCatChem* **2015**, *7*, 2508–2516. [CrossRef]
39. Rauta, P.R.; Manivasakan, P.; Rajendran, V.; Sahu, B.B.; Panda, B.K.; Mohapatra, P. Phase transformation of ZrO_2 nanoparticles produced from zircon. *Phase Transit.* **2012**, *85*, 13–26. [CrossRef]

40. Xu, Y.; Du, X.-H.; Li, J.; Wang, P.; Zhu, J.; Ge, F.-J.; Zhou, J.; Song, M.; Zhu, W.-Y. A comparison of Al_2O_3 and SiO_2 supported Ni-based catalysts in their performance for the dry reforming of methane. *J. Fuel Chem. Technol.* **2019**, *47*, 199–208. [CrossRef]
41. Liu, W.; Li, L.; Zhang, X.; Wang, Z.; Wang, X.; Peng, H. Design of Ni-ZrO_2@SiO_2 catalyst with ultra-high sintering and coking resistance for dry reforming of methane to prepare syngas. *J. CO2 Util.* **2018**, *27*, 297–307. [CrossRef]
42. Kauppi, E.I.; Honkala, K.; Krause, A.O.I.; Kanervo, J.M.; Lefferts, L. ZrO_2 Acting as a Redox Catalyst. *Top. Catal.* **2016**, *59*, 823–832. [CrossRef]
43. Santamaria, L.; Arregi, A.; Alvarez, J.; Artetxe, M.; Amutio, M.; Lopez, G.; Bilbao, J.; Olazar, M. Performance of a Ni/ZrO_2 catalyst in the steam reforming of the volatiles derived from biomass pyrolysis. *J. Anal. Appl. Pyrolysis* **2018**, *136*, 222–231. [CrossRef]
44. Zhang, M.; Zhang, J.; Wu, Y.; Pan, J.; Zhang, Q.; Tan, Y.; Han, Y. Insight into the effects of the oxygen species over Ni/ZrO_2 catalyst surface on methane reforming with carbon dioxide. *Appl. Catal. B Environ.* **2019**, *244*, 427–437. [CrossRef]
45. Wang, X.; Bai, X.; Guo, Y.; Liu, Q.; Ji, S.; Wang, Z.J. A nanoscale Ni/ ZrO_2 catalyst coated with Al_2O_3 for carbon dioxide reforming of methane. *J. Chem. Technol. Biotechnol.* **2021**, *96*, 474–480. [CrossRef]
46. Sangsong, S.; Ratana, T.; Tungkamani, S.; Sornchamni, T.; Phongaksorn, M. Effect of CeO_2 loading of the Ce-Al mixed oxide on ultrahigh temperature water-gas shift performance over Ce-Al mixed oxide supported Ni catalysts. *Fuel* **2019**, *252*, 488–495. [CrossRef]
47. Chen, L.; Qi, Z.; Zhang, S.; Su, J.; Somorjai, G.A. Catalytic Hydrogen Production from Methane: A Review on Recent Progress and Prospect. *Catalysts* **2020**, *10*, 858. [CrossRef]
48. Nabgan, W.; Nabgan, B.; Abdullah, T.A.T.; Ngadi, N.; Jalil, A.A.; Hassan, N.S.; Izan, S.M.; Luing, W.S.; Abdullah, S.N.; Majeed, F.S.A. Conversion of polyethylene terephthalate plastic waste and phenol steam reforming to hydrogen and valuable liquid fuel: Synthesis effect of Ni–Co/ZrO_2 nanostructured catalysts. *Int. J. Hydrogen Energy* **2020**, *45*, 6302–6317. [CrossRef]
49. Vrijburg, W.L.; Van Helden, J.W.A.; Parastaev, A.; Groeneveld, E.; Pidko, E.A.; Hensen, E.J.M. Ceria–zirconia encapsulated Ni nanoparticles for CO_2 methanation. *Catal. Sci. Technol.* **2019**, *9*, 5001–5010. [CrossRef]
50. Dharmasaroja, N.; Ratana, T.; Tungkamani, S.; Sornchamni, T.; Simakov, S.A.; Phongaksorn, M. Catalysts and the Performance of the Ni/Al_2O_3-MgO Catalyst for the Combined Steam and CO_2 Reforming of Methane Using Ultra-Low Steam to Carbon Ratio. *Catalysts* **2020**, *10*, 1450. [CrossRef]